Research Article | Vol. 27, No. 24 / 25 November 2019 / Optics Express 34611
Optics EXPRESS

Generation and characterization of position-momentum entangled photon pairs in a hot atomic gas cell

CHENGYUAN WANG,[1,2,4] CHUNG-HYUN LEE,[2] AND YOON-HO KIM[2,3]

[1] *Shaanxi Key Laboratory of Quantum Information and Quantum Optoelectronic Devices, School of Science, Xi'an Jiaotong University, Xi'an, 710049, China*
[2] *Department of Physics, Pohang University of Science and Technology (POSTECH), Pohang, 37673, South Korea*
[3] *yoonho72@gmail.com*
[4] *wcy199202@gmail.com*

Abstract: Continuous-variable position-momentum entanglement (or Einstein-Podolsky-Rosen entanglement) of two particles has played important roles in the fundamental study of quantum physics as well as in the progress of quantum information. In this paper, we propose a scheme to generate Einstein-Podolsky-Rosen (EPR) position-momentum entangled photon pairs efficiently via spontaneous four-wave mixing (SFWM) process in a hot rubidium gas cell. The EPR entanglement between the photon pair is measured and characterized by using the ghost interference and the ghost imaging method. Due to the simplicity of the experimental setup and the high photon pair generation rate, our EPR entangled photon source may has potential applications in quantum imaging, hyperentanglement preparation and atomic ensemble based quantum information processing and quantum communication protocols.

1. Introduction

Einstein-Podolsky-Rosen (EPR) entanglement was initially proposed in an attempt to argue the incompleteness of quantum theory [1]. This EPR gedanken experiment involved two particles that are entangled in their positions and momenta such that the product of variance of position difference and variance of momentum sum violates the Heisenberg inequality. Although initially proposed for the position-momentum variable, studies on continuous variable bipartite EPR entanglement have largely involved in measuring the field quadratures [2–7]. EPR entanglement has been well studied in recent years not only for better understanding of quantum physics but also for its potential applications in the fields of quantum imaging, quantum metrology and quantum computation [8–12], etc.

Genuine position and momentum EPR entangled photons were firstly generated by spontaneous parametric down-conversion (SPDC) process in crystals [16–19]. Later it was shown that position and momentum entangled photons with narrow bandwidth can be generated via spontaneous four-wave mixing (SFWM) in cold atom ensembles [20]. The atoms inside the crystals and cold atomic ensembles are almost motionless, which makes them ideal mediums to generate position and momentum entangled photons since the quality of photon entanglement will not be degraded by the atomic motion. But the SPDC photon's bandwidth is too broad to be directly utilized in light-atom interaction based quantum communication protocols while the cold atom system is bulky and difficult to operate. Recently, photon pairs generated via SFWM in hot atomic ensembles [21–24] attracted lots of attention due to easy realization and the narrow bandwidth features. Whether the hot atomic gas cell is able to generate high quality position and momentum EPR entangled photon pairs has not been reported yet.

#376447 https://doi.org/10.1364/OE.27.034611
Journal © 2019 Received 28 Aug 2019; revised 2 Nov 2019; accepted 3 Nov 2019; published 11 Nov 2019

Optics EXPRESS

In this paper, we exhibit the first experimental realization of high brightness EPR entangled photon pairs via ladder type SFWM in a hot ^{87}Rb gas cell. The EPR position momentum entanglement is verified by quantum ghost interference and ghost imaging method [18,20], and the results show that the biphotons satisfy the inseparability criterion as well as the EPR steering criterion. The photon's bandwidth is much narrower than the SPDC source and the experimental requirements are greatly simplified compared with cold atom system, hence our position and momentum EPR entangled photon source can be widely applied to the atomic ensemble based quantum information processing and quantum communication protocols [13–15].

2. Experimental results and discussions

The experimental setup is shown in Fig. 1. The vertically polarized pump and coupling beams counter propagate through a 20 mm long ^{87}Rb vapor cell, which is heated to 65 °C. The pump beam (780 nm, ω_p) is blue detuned from $|5S_{1/2}, F = 2\rangle \rightarrow |5P_{3/2}, F' = 3\rangle$ by 1 GHz, while the coupling beam (776 nm, ω_c) is red detuned from $|5P_{3/2}, F' = 3\rangle \rightarrow |5D_{5/2}, F'' = 4\rangle$ by 1 GHz. The ω_p and ω_c here are both collimated beams with $1/e^2$ beam diameters of 1700 μm. The powers are 1.3 mW for ω_p and 12 mW for ω_c beam. The horizontally polarized anti-Stokes photons (776 nm, ω_{as}) and Stokes photons (780 nm, ω_s) are collected with an angle of 1.2° relative to ω_p and ω_c. SFWM with this energy level scheme can generate photon-pair source with high brightness comparable to that of SPDC while the photon bandwidth is much narrower than SPDC [25,26]. Figure 2 is the measured coincidence counts between ω_{as} and ω_s photons, which shows that the maximum cross correlation function $G^{(2)}_{as,s}(\tau)$ can reach up to 11,000 with 60 s collection time (the time resolution of our coincidence detection system is 162 ps). The full width at half maximum (FWHM) of $G^{(2)}_{as,s}(\tau)$ from Fig. 2 is about 2 ns, corresponding to the biphoton bandwidth of 500 MHz. Photon pair's generation rate is estimated as 6,000 pairs/s (considering all of the losses terms, i. e. the total fiber-fiber coupling efficiency of 70%, the filters transmission efficiency of 80% and single photon counting module detection efficiency of 50%). The EPR entanglement between the photon pair is measured and characterized by using the ghost interference and the ghost imaging method [18,20], which will be exclusively described below.

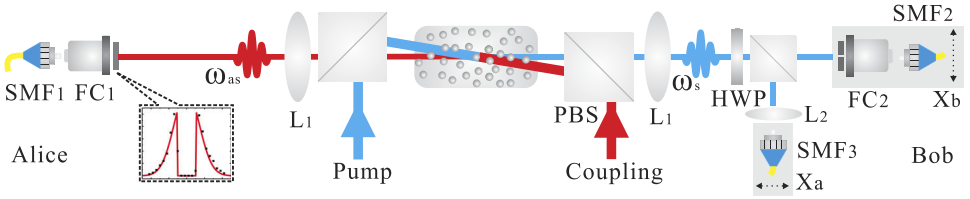

Fig. 1. Sketch of experimental setup. EPR position-momentum entanglement photon pairs are generated via ladder type SFWM in a 20 mm long ^{87}Rb atomic gas cell. Dashed inset: profile of an effective double slit when a collimated Gaussian beam passes through 1 mm plastic block. (SMF, single mode fiber; FC, fiber collimator; PBS, polarizing beam splitter; HWP, half-wave plate; L_1, lenses with focal length of f_1 = 300 mm; L_2, lens with focal length of f_2 = 35 mm; $X_{a(b)}$ is the transverse position of $SMF_{3(2)}$.

Classical momentum-correlated or position-correlated photon pairs can realize ghost interference or ghost imaging, but it is impossible to obtain both with the same prepared photon pair state due to the uncertainty principle [18]. So in this paper we verify that our photon pairs are EPR entangled by observing high visibility ghost interference and high contrast ghost imaging.

Ghost interference and ghost imaging have been studied extensively in recent years [28–30]. Generally, when the paired photons are used for observing ghost interference or ghost imaging, one photon passes through an object and is collected by a bucket detector with no spatial

Optics EXPRESS

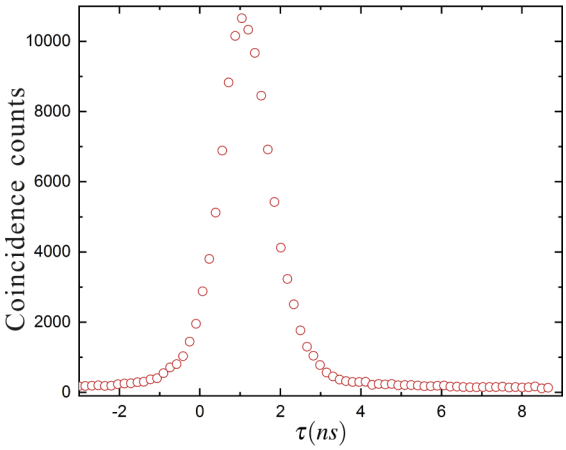

Fig. 2. The coincidence counts between ω_{as} and ω_s photons with 60 s collection time. The horizontal coordinate is the relative time delay between ω_{as} and ω_s photons and vertical coordinate is the cross correlation function $G^{(2)}_{as,s}(\tau)$.

resolution, while the other photon is recorded by another detector with spatial resolution in the near field or far field. Coincidence counts between this two detectors will reveal ghost imaging or ghost interference.

Before the experiment we align the optical path with a coherent Gaussian beam, which comes out from SMF_1 and is collimated by FC_1. An opaque plastic block with 1 mm width is attached to the center of FC_1, which is equivalent to an effective double slit when the collimated Gaussian beam passes through it. A narrow vertical slit with 0.4 mm width attached to the center of FC_2 and together with SMF_2 are mounted on a translation stage (TS), which compose the ghost imaging measurement setup. The SMF_3 fixed on the other TS is used for ghost interference measurement. The center of the atomic vapor cell is located at the focus of the two lenses L_1. FC_1, FC_2 and L_2 are also placed at the focus of the lenses L_1. Hence these two L_1 can form a 4-f system and the double slit can be imaged from FC_1 to the positions of FC_2 and L_2. So if the optical path is aligned well, a clear classical image of the double slit can be obtained by scanning the ghost imaging measurement setup. We record the relative intensity collected by SMF_2 against the transverse position of the ghost imaging measurement setup, as shown inside the dashed label in Fig. 1 with black dots. The red line is the theoretical curve from the product of the opaque plastic block and Gaussian envelope, which clearly reveals a profile of double slit. Also, a double slit interference pattern should be observed by scanning the SMF_3 at the focus of L_2.

After this step we start on the ghost interference and ghost imaging measurement. The ω_p and ω_c beams here are both collimated with $1/e^2$ diameters of 1700 μm. ω_{as} photons are collected by FC_1 after passing through the block and coupled into the fixed SMF_1 on Alice's side while ω_s photons go to Bob's direction. A HWP and a PBS on Bob's side decide whether to conduct ghost interference (HWP at 45°) or ghost imaging (HWP at 0°) measurement. For the ghost interference experiment, ω_s photons are coupled into SMF_3 which is scanned at the focus of L_2. The normalized coincidence counts between ω_{as} and ω_s photons are recorded against the transverse position X_a with 60 s collection time, as shown in Fig. 3(a). The result shows a clear ghost interference pattern. For the ghost imaging measurement, ω_{as} photons are collected by SMF_2 and the normalized coincidence counts between ω_{as} and ω_s photons are recorded against the transverse position X_b with 80 s collection time, as shown in Fig. 3(e). The ghost imaging result reveals the profile of the effective double slit. Observation of high visibility

Optics EXPRESS

ghost interference and high contrast ghost imaging confirms that our photon pairs are EPR position-momentum entangled.

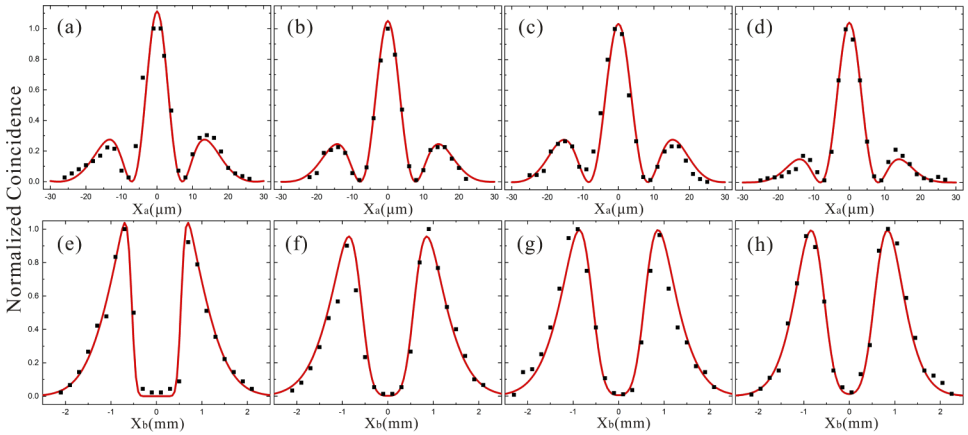

Fig. 3. Experimental results for ghost interference (a)-(d) and ghost imaging (e)-(h). The $1/e^2$ pump beam diameter at the center of the vapor cell from (a)-(d) and (e)-(h) is 1700 μm, 1000 μm, 500 μm, 330 μm, respectively. Each point of the experimental data is accumulated of 60(80) s for the ghost interference (ghost imaging) measurement. The black dots are normalized coincidence counts after subtracting the uncorrelated noise while the red curves come from theoretical fitting.

Basically large pump beam size can guarantee high quality of EPR entanglement. But in real situations small experimental beam size is helpful for spatially filtering noise, increasing light intensity or for other purposes such as [32]. So we also check the influence of beam size on the EPR entanglement performance by changing the pump beam waist to 1700 μm, 1000 μm, 500 μm and 330 μm while fixing the coupling beam size at 1700 μm. The results are shown in Fig. 3(a)–3(d) and 3(e)–3(h) for ghost interference and ghost imaging respectively. From the results we can see that the quality of ghost interference and ghost imaging drops with the decrement of pump beam size, but all the results show clear ghost interference and ghost imaging patterns.

In the following we will compare the results with theoretical fitting. For the ghost interference and ghost imaging measurement, the normalized coincidence counts can be calculated by [20,27]

$$G^{(2)}(\vec{X}_a) = \left| \int d\vec{\kappa}_s d\vec{\kappa}_{as} \tilde{\mathcal{E}}_+ \left(|\vec{\kappa}_+|\right) \tilde{\mathcal{E}}_- \left(|\vec{\kappa}_-|/2\right) \mathcal{T}\left(\frac{\lambda_{as} f_1}{2\pi}\vec{\kappa}_{as}\right) \exp\left(-i\frac{f_1}{f_2}\vec{\kappa}_s \cdot \vec{X}_a\right) \right|^2 \tag{1}$$

$$G^{(2)}(\vec{X}_b) = \left| \int d\vec{\kappa}_s d\vec{\kappa}_{as} \tilde{\mathcal{E}}_+ \left(|\vec{\kappa}_+|\right) \tilde{\mathcal{E}}_- \left(|\vec{\kappa}_-|/2\right) \mathcal{T}\left(\frac{\lambda_{as} f_1}{2\pi}\vec{\kappa}_{as}\right) \times \delta\left(\vec{\kappa}_s - \frac{\omega_s}{c f_1}\vec{X}_b\right) \right|^2 \tag{2}$$

Here $\tilde{\mathcal{E}}_\pm$ are Gaussian envelopes with standard deviations $\sigma_\pm$. $\vec{\kappa}_\pm = \vec{\kappa}_s \pm \vec{\kappa}_{as}$ represent the wave vectors. $\mathcal{T}(\vec{X}_o)$ is the object transfer function of the double slit.

In the ideal case, supposing the pump and coupling beams are plane waves such that $\tilde{\mathcal{E}}_+ \left(|\vec{\kappa}_+|\right) = \delta\left(\vec{\kappa}_+\right)$ and $\tilde{\mathcal{E}}_- \left(|\vec{\kappa}_-|\right) = 1$. Then $G^{(2)}(\vec{X}_a)$ is simplified as $\left|\tilde{\mathcal{T}}\left[(f_1/f_2)\,\vec{\rho}_b\right]\right|^2$, which is the Fourier transform of the object transfer function and exhibits an interference envelop. While $G^{(2)}(\vec{X}_b)$ is proportional to $|\mathcal{T}(-\vec{X}_b)|^2$ and reveals the shape of the double slit. But under the real experimental conditions, pump beam waist has finite size such that $\tilde{\mathcal{E}}_+ \left(|\vec{\kappa}_+|\right) \tilde{\mathcal{E}}_- \left(|\vec{\kappa}_-|/2\right) \neq \delta\left(\vec{\kappa}_+\right)$. Hence the ghost interference and ghost imaging results, which depend on σ_+ and σ_-, will suffer deviations from the ideal cases. Thus the values of σ_+ and σ_- can be obtained by fitting the

Optics EXPRESS

coincidence envelops of the non-ideal ghost interference and ghost imaging with theory. Then the uncertainty of the total momentum sum $\Delta p_+ = \Delta(\vec{p}_s + \vec{p}_{as}) = \hbar\sigma_+/\sqrt{2}$ and the uncertainty of the position difference $\Delta x_- = \Delta(\vec{x}_{as} - \vec{x}_s) = \sigma_-^{-1}/\sqrt{2}$ can be calculated correspondingly.

The ideal EPR-entangled photon pairs, such as $\Delta x_- = \Delta\left(\vec{x}_{as} - \vec{x}_s\right) = 0$ and $\Delta p_+ = \Delta\left(\vec{p}_s + \vec{p}_{as}\right) = 0$, are impossible to be obtained under real experimental conditions. Basically, biphotons are EPR entangled if they satisfy the inseparability criterion

$$\left\langle (\Delta x_-)^2 \right\rangle \left\langle (\Delta p_+)^2 \right\rangle < \hbar^2 \tag{3}$$

Another striker criterion to judge whether the EPR paradox occurs is the EPR steering criterion

$$\left\langle (\Delta x_-)^2 \right\rangle \left\langle (\Delta p_+)^2 \right\rangle < \hbar^2/4 \tag{4}$$

Quantum correlations can be classified into different regimes by this two criterions, as has been shown in [31].

By fitting experimental data in Fig. 3(a)–3(h) with the theory we can obtain the corresponding values of $\left\langle (\Delta x_-)^2 \right\rangle \left\langle (\Delta p_+)^2 \right\rangle$, which are shown in Table 1. From Table 1, we can see that with the decrease of pump beam size, $\left\langle (\Delta x_-)^2 \right\rangle \left\langle (\Delta p_+)^2 \right\rangle$ in unit of $\hbar^2$ declines both in the ghost interference and ghost imaging cases. But all the results satisfy the inseparability criterion in Eq. (3) as well as the EPR steering criterion in Eq. (4). This confirms that the photon pairs generated by SFWM in the hot atomic vapor cell are EPR position-momentum entangled. The outcomes also show that under certain focused pump beam size, EPR position-momentum entanglement still exists. This property can be combined with [32] to generate versatile photon pairs.

Table 1. $\left\langle (\Delta x_-)^2 \right\rangle \left\langle (\Delta p_+)^2 \right\rangle$ in unit of $\hbar^2$ with different pump beam size

Pump size (μm)	1700	1000	500	330
Ghost interference	0.0011	0.0069	0.0204	0.0232
Ghost imaging	0.0004	0.0016	0.0025	0.0077

3. Conclusion

In conclusion, we demonstrate a scheme to efficiently generate EPR position-momentum entangled photon pairs via ladder type SFWM in the hot vapor cell. The EPR entanglement between the photon pair is measured and characterized by using the ghost interference and the ghost imaging method. By fitting the experimental data with theory we show that our EPR entangled photon pair source satisfies the inseparability criterion as well as the EPR steering criterion. We also study the influence of pump beam size on the EPR entanglement properties. Such EPR entangled photon pair source can have high brightness comparable to that of SPDC while the photon bandwidth is much narrower than SPDC [25]. The system size and operating difficulty based on hot atoms are greatly simplified compared with cold atoms [20,33]. Our EPR entangled photon pair source may have potential applications in quantum imaging, continuous-variable (CV) entanglement based quantum teleportation, quantum key distribution and light-atom interaction based quantum communication protocols. Besides, EPR entanglement can be combined with other degrees of freedom entanglement [34–37] to generate hyper-entanglement state, which may have broad applications in quantum information processing.

Funding

National Research Foundation of Korea (2019R1A2C3004812); National Natural Science Foundation of China (11534008, 11774286).

Optics EXPRESS

References

1. A. Einstein, B. Podolsky, and N. Rosen, "Can Quantum-Mechanical Description of Physical Reality Be Considered Complete?" Phys. Rev. **47**(10), 777–780 (1935).
2. Z. Y. Ou, S. F. Pereira, H. J. Kimble, and K. C. Peng, "Realization of the Einstein-Podolsky-Rosen paradox for continuous variables," Phys. Rev. Lett. **68**(25), 3663–3666 (1992).
3. W. P. Bowen, R. Schnabel, P. K. Lam, and T. C. Ralph, "Experimental characterization of continuous-variable entanglement," Phys. Rev. A **69**(1), 012304 (2004).
4. T. Eberle, V. Händchen, J. Duhme, T. Franz, R. F. Werner, and R. Schnabel, "Strong Einstein-Podolsky-Rosen entanglement from a single squeezed light source," Phys. Rev. A **83**(5), 052329 (2011).
5. A. M. Marino, R. C. Pooser, V. Boyer, and P. D. Lett, "Tunable delay of Einstein-Podolsky-Rosen entanglement," Nature **457**(7231), 859–862 (2009).
6. J. Li, S.-Y. Zhu, and G. S. Agarwal, "Magnon-Photon-Phonon Entanglement in Cavity Magnomechanics," Phys. Rev. Lett. **121**(20), 203601 (2018).
7. Z. Zhang, M. O. Scully, and G. S. Agarwal, "Quantum entanglement between two magnon modes via Kerr nonlinearity driven far from equilibrium," Phys. Rev. Research **1**(2), 023021 (2019).
8. K. Wagner, J. Janousek, V. Delaubert, H. Zou, C. Harb, N. Treps, J. F. Morizur, P. K. Lam, and H. A. Bachor, "Entangling the Spatial Properties of Laser Beams," Science **321**(5888), 541–543 (2008).
9. G. Brida, M. Genovese, and I. Ruo Berchera, "Experimental realization of sub-shot-noise quantum imaging," Nat. Photonics **4**(4), 227–230 (2010).
10. T. Ono, R. Okamoto, and S. Takeuchi, "An entanglement-enhanced microscope," Nat. Commun. **4**(1), 2426 (2013).
11. D. S. Tasca, R. M. Gomes, F. Toscano, P. H. Souto Ribeiro, and S. P. Walborn, "Continuous-variable quantum computation with spatial degrees of freedom of photons," Phys. Rev. A **83**(5), 052325 (2011).
12. M. D. Reid, P. D. Drummond, W. P. Bowen, E. G. Cavalcanti, P. K. Lam, H. A. Bachor, U. L. Andersen, and G. Leuchs, "The Einstein-Podolsky-Rosen paradox: From concepts to applications," Rev. Mod. Phys. **81**(4), 1727–1751 (2009).
13. M. Dabrowski, M. Parniak, and W. Wasilewski, "Einstein-Podolsky-Rosen paradox in a hybrid bipartite system," Optica **4**(2), 272 (2017).
14. M. Dabrowski, M. Mazelanik, M. Parniak, A. Leszczyński, M. Lipka, and W. Wasilewski, "Certification of high-dimensional entanglement and Einstein-Podolsky-Rosen steering with cold atomic quantum memory," Phys. Rev. A **98**(4), 042126 (2018).
15. W. Zhang, M.-X. Dong, D.-S. Ding, S. Shi, K. Wang, S.-L. Liu, Z.-Y. Zhou, G.-C. Guo, and B.-S. Shi, "Einstein-Podolsky-Rosen entanglement between separated atomic ensembles," Phys. Rev. A **100**(1), 012347 (2019).
16. T. B. Pittman, Y. H. Shih, D. V. Strekalov, and A. V. Sergienko, "Optical imaging by means of two-photon quantum entanglement," Phys. Rev. A **52**(5), R3429–R3432 (1995).
17. D. V. Strekalov, A. V. Sergienko, D. N. Klyshko, and Y. H. Shih, "Observation of Two-Photon "Ghost" Interference and Diffraction," Phys. Rev. Lett. **74**(18), 3600–3603 (1995).
18. M. D'Angelo, Y.-H. Kim, S. P. Kulik, and Y. Shih, "Identifying entanglement using quantum ghost interference and imaging," Phys. Rev. Lett. **92**(23), 233601 (2004).
19. J. C. Howell, R. S. Bennink, S. J. Bentley, and R. W. Boyd, "Realization of the Einstein-Podolsky-Rosen Paradox Using Momentum- and Position-Entangled Photons from Spontaneous Parametric Down Conversion," Phys. Rev. Lett. **92**(21), 210403 (2004).
20. J.-C. Lee, K.-K. Park, T.-M. Zhao, and Y.-H. Kim, "Einstein-Podolsky-Rosen Entanglement of Narrow-Band Photons from Cold Atoms," Phys. Rev. Lett. **117**(25), 250501 (2016).
21. D.-S. Ding, Z.-Y. Zhou, B.-S. Shi, X.-B. Zou, and G.-C. Guo, "Generation of non-classical correlated photon pairs via a ladder-type atomic configuration: theory and experiment," Opt. Express **20**(10), 11433 (2012).
22. C. Shu, P. Chen, T. K. A. Chow, L. Zhu, Y. Xiao, M. M. T. Loy, and S. Du, "Subnatural-linewidth biphotons from a Doppler-broadened hot atomic vapor cell," Nat. Commun. **7**(1), 12783 (2016).
23. L. Podhora, P. Obšil, I. Straka, M. Ježek, and L. Slodička, "Nonclassical photon pairs from warm atomic vapor using a single driving laser," Opt. Express **25**(25), 31230 (2017).
24. C. Wang, Y. Gu, Y. Yu, D. Wei, P. Zhang, H. Gao, and F. Li, "Efficient generation of non-classical photon pairs in a hot atomic ensemble," Chin. Opt. Lett. **16**(8), 082701 (2018).
25. Y.-S. Lee, S. M. Lee, H. Kim, and H. S. Moon, "Highly bright photon-pair generation in Doppler-broadened ladder-type atomic system," Opt. Express **24**(24), 28083 (2016).
26. J. Park, T. Jeong, H. Kim, and H. S. Moon, "Time-Energy Entangled Photon Pairs from Doppler-Broadened Atomic Ensemble via Collective Two-Photon Coherence," Phys. Rev. Lett. **121**(26), 263601 (2018).
27. M. D'Angelo, A. Valencia, M. H. Rubin, and Y. Shih, "Resolution of quantum and classical ghost imaging," Phys. Rev. A **72**(1), 013810 (2005).
28. Y. Yu, C. Wang, J. Liu, J. Wang, M. Cao, D. Wei, H. Gao, and F. Li, "Ghost imaging with different frequencies through non-degenerated four-wave mixing," Opt. Express **24**(16), 18290 (2016).
29. D.-S. Ding, Z.-Y. Zhou, B.-S. Shi, X.-B. Zou, and G.-C. Guo, "Two-color ghost interference with photon pairs generated in hot atoms," AIP Adv. **2**(3), 032177 (2012).
30. D.-G. Im, Y. Kim, and Y.-H. Kim, "Periodic revival of frustrated two-photon creation via interference," Opt. Express **27**(5), 7593 (2019).

Optics EXPRESS

31. H. M. Wiseman, S. J. Jones, and A. C. Doherty, "Steering, Entanglement, Nonlocality, and the Einstein-Podolsky-Rosen Paradox," Phys. Rev. Lett. **98**(14), 140402 (2007).
32. L. Zhao, X. Guo, Y. Sun, Y. Su, M. M. T. Loy, and S. Du, "Shaping the Biphoton Temporal Waveform with Spatial Light Modulation," Phys. Rev. Lett. **115**(19), 193601 (2015).
33. K.-K. Park, Y.-W. Cho, Y.-T. Chough, and Y.-H. Kim, "Experimental Demonstration of Quantum Stationary Light Pulses in an Atomic Ensemble," Phys. Rev. X **8**(2), 021016 (2018).
34. J. Park, H. Kim, and H. S. Moon, "Polarization-Entangled Photons from a Warm Atomic Ensemble Using a Sagnac Interferometer," Phys. Rev. Lett. **122**(14), 143601 (2019).
35. T.-M. Zhao, Y. S. Ihn, and Y.-H. Kim, "Direct Generation of Narrow-band Hyperentangled Photons," Phys. Rev. Lett. **122**(12), 123607 (2019).
36. H. Yan, S. Zhang, J. F. Chen, M. M. T. Loy, G. K. L. Wong, and S. Du, "Generation of narrow-band hyperentangled nondegenerate paired photons," Phys. Rev. Lett. **106**(3), 033601 (2011).
37. S. Shi, D. S. Ding, Y. C. Yu, W. Zhang, M.-X. Dong, K. Wang, Y. H. Ye, G. C. Guo, and B. S. Shi, "Vortex-phase-dependent momentum and position entanglement generated from cold atoms," Phys. Rev. A **97**(6), 063847 (2018).